Coupling of Neutral-Beam-Driven Compressional Alfvén Eigenmodes to Kinetic Alfvén Waves in NSTX Tokamak and Energy Channeling

E. V. Belova,[*] N. N. Gorelenkov, E. D. Fredrickson, and K. Tritz

Princeton Plasma Physics Laboratory, P. O. Box 451, Princeton, New Jersey 08543, USA

N. A. Crocker

University of California, Los Angeles, California 90095, USA

An energy-channeling mechanism is proposed to explain flattening of the electron temperature profiles at a high beam power in the beam-heated National Spherical Torus Experiment (NSTX). Results of self-consistent simulations of neutral-beam-driven compressional Alfvén eigenmodes (CAEs) in NSTX are presented that demonstrate strong coupling of CAEs to kinetic Alfvén waves at the Alfvén resonance location. It is suggested that CAEs can channel energy from the beam ions to the location of the resonant mode conversion at the edge of the beam density profile, modifying the energy deposition profile.

Flattening of electron temperature profiles and anomalously low central temperatures at a high beam power in the National Spherical Torus Experiment (NSTX) have been linked with strong activity of Alfvén modes in a subcyclotron frequency range [1,2]. The reduced heating of the plasma center in NSTX can significantly limit plasma performance, and can potentially have important implications for future fusion devices, especially low-aspect-ratio tokamaks. Modes in a frequency range between 0.1 and 1.0 of the ion cyclotron frequency are often observed during neutral beam injection in NSTX; they were identified as compressional Alfvén eigenmodes (CAEs) and global Alfvén eigenmodes (GAEs), driven unstable through the resonance with the super Alfvénic beam ions [3,4]. The GAE in toroidal geometry is characterized by shear Alfvén wave polarization and frequency below the minimum of the Alfvén continuum [5–7], and the CAE is a fast magnetosonic eigenmode [8]. Previous theoretical studies attributed the flattening of the electron temperature profile to an enhanced electron transport due to these modes. Several mechanisms have been suggested, including the interaction of Alfvén eigenmodes with bulk electrons via parallel electric field as well as stochasticity of the electron orbits in the presence of multiple unstable and overlapping modes of sufficiently large amplitudes [9]. However, other estimates [10] suggest that Alfvén-eigenmode-induced transport should have a minor effect, but that the energy channeling from center-localized GAEs to continuum damping closer to the edge can be responsible for the observed flattening of the electron temperature profiles. This Letter presents the first self-consistent simulations of neutral-beam-driven compressional Alfvén eigenmodes demonstrating an important alternative: an energy-channeling mechanism that will occur for any unstable CAE in NSTX. Three-dimensional hybrid magnetohydrodynamics (MHD)-particle simulations show that an essential feature of CAE modes in toroidal geometry is

their coupling to kinetic Alfvén waves (KAWs), which occurs at the Alfvén resonance location. The beam-driven CAE can mode convert to KAW, channeling energy from the beam ions at the injection region near the magnetic axis to the location of the resonant mode conversion at the edge of the beam density profile. This mechanism can explain the reduced heating of the plasma center in NSTX. It is also shown that strong CAE/KAW coupling follows from the dispersion relation, and will occur for any unstable compressional mode. In this Letter, a numerical model and the results of linearized and fully nonlinear simulations are described, focusing on CAE/KAW properties, and possible effects of CAE/KAW coupling on the electron temperature profiles in the NSTX are discussed.

The hybrid code HYM [11–13] has been used to investigate properties of beam-ion-driven compressional Alfvén eigenmodes in NSTX. The HYM code is a 3D nonlinear global stability code in toroidal geometry, which treats the beam ions using full-orbit, delta-f particle simulations, while the one-fluid resistive MHD model is used to represent the background plasma. The two plasma components are coupled using a current coupling scheme. In this scheme, the momentum equation for the thermal plasma is $\rho d\mathbf{V}/dt = -\nabla p + (\mathbf{J} - \mathbf{J}_b) \times \mathbf{B}/c - qn_b\mathbf{E} + \nu\Delta\mathbf{V}$ where ρ, $\mathbf{V}$, and p are the thermal plasma density, velocity, and pressure; n_b and $\mathbf{J}_b$ are the beam ion density and the beam-ion-induced current, ν is a viscosity coefficient, and $\mathbf{J}$ is the total plasma current. It is assumed that the fast-ion pressure can be comparable to that of the thermal plasma, but the beam ions have a low density $n_b \ll n_e$. In this case, the MHD Ohm's law applies: $\mathbf{E} = -\mathbf{V} \times \mathbf{B}/c + \eta\mathbf{J}$. The delta-$f$ method is used to reduce numerical noise in the simulations. In this method, the equilibrium distribution function of beam ions needs to be known analytically, and the equation for the perturbed distribution function

$\delta F = F - F_0$ is integrated along the particle trajectories. Equilibrium distribution function is taken to be in the form [14] $F_0 = F_1(v)F_2(\lambda)F_3(p_\phi)$, where $v = \sqrt{2\varepsilon/m_i}$ is the particle velocity, $\lambda \equiv \mu B_0/\varepsilon$ is the pitch-angle variable, $p_\phi = -\psi + Rv_\phi$, and functions $F_{1,2,3}$ are defined by

$$F_1(v) = 1/(v^3 + v_*^3), \quad \text{for } v < v_0, \qquad (1)$$

$$F_2(\lambda) = C \exp(-(\lambda - \lambda_0)^2/\Delta\lambda^2), \qquad (2)$$

$$F_3(p_\phi) = [(p_\phi - p_{\min})/(p_{\max} - p_{\min})]^\alpha, \quad \text{for } p_\phi > p_{\min}, \qquad (3)$$

where $F_0 = 0$ for $v > v_0$ or $p_\phi < p_{\min}$, v_0 is the injection velocity, and we assumed $v_* = v_0/2$. The parameters for the pitch-angle distribution are $\Delta\lambda = 0.3$ and $\lambda_0 = 0.7$. The function $F_3(p_\phi)$ is used to match the TRANSP profiles of the beam-ion density, where $\alpha = 6$ is a numerical parameter, and the condition $p_\phi > p_{\min}$ describes a prompt-loss boundary. A generalized form of the Grad-Shafranov equation solver has been developed, which includes, nonperturbatively, the effects of the beam ions with anisotropic distribution [14].

The excitation of compressional Alfvén eigenmodes has been studied for the high-confinement-regime plasma of NSTX shot 141398, and equilibrium profiles and plasma parameters have been chosen to match magnetic-field and plasma profiles for this shot using the TRANSP and EFIT codes. Plasma was heated by 6 MW of 90-keV deuterium beams with $n_b = 3.5 \times 10^{18}$ m^{-3}, $n_e = 6.7 \times 10^{19}$ m^{-3}, $B_t = 0.325T$, $I_p = 0.8$ MA, and $v_0 = 4.9V_A$. In this shot, significant Alfvén mode activity has been observed, and detailed measurements of amplitudes and mode structures were obtained [2,15]. The observed modes have been identified, based on dispersion relations, as compressional Alfvén eigenmodes for frequencies $f > 600$ kHz and small toroidal mode numbers $|n| < 6$, and as global Alfvén eigenmodes for $f < 600$ kHz and $|n| \sim 6-8$ [2,15]. Compressional Alfvén eigenmodes with higher toroidal mode numbers $n > 8$ have also been observed in this shot [16].

Simulations for this case show that the most unstable modes for $n = 5$–7 are GAEs with frequencies $\omega/\omega_{ci} = 0.15$–0.22 ($f = 380$–550 kHz). The most unstable modes for $n = 4$ and $n = 8, 9$ are CAEs, which have been identified based on the calculated large compressional component of perturbed magnetic field, and have higher frequencies $\omega/\omega_{ci} = 0.35$–0.5 ($f = 870$–1200 kHz). Here all frequencies are normalized to the ion cyclotron frequency at the axis $f_{ci} = 2.5$ MHz. The calculated range of the unstable toroidal mode numbers, frequencies, and mode polarizations appear to be reasonably close to experimental observations [2,15]. More detailed comparisons of the mode frequencies and structure with experimental data will be performed in the future.

In NSTX, the CAEs are driven unstable by the resonant interaction with the beam ions. Numerical analysis of the resonant wave-particle interaction for the $n = 8$ CAE simulation shows two separate groups of resonant particles: one group satisfying the regular resonance condition $\omega - k_\parallel v_\parallel = 0$, and a group of higher-energy particles satisfying the Doppler-shifted cyclotron resonant condition $\omega - k_\parallel v_\parallel + \omega_{ci} = 0$. It was found that the main contribution to the instability drive comes from the beam ions with parallel velocity comparable to the phase velocity of the CAE; the contribution from the cyclotron resonances is negligible.

Figure 1 shows poloidal contour plots of the perturbed magnetic field for the $n = 8$ ($\omega = 0.48\omega_{ci}$) and the $n = 4$ ($\omega = 0.35\omega_{ci}$) CAEs. Here R is major radius, and the magnetic axis is located approximately at $R = 1.1$ m. It can be seen that the CAEs are localized near the magnetic axis, where they have mostly compressional polarization, and $\delta B_\parallel$ is significantly larger than $\delta B_\perp$ everywhere, except in the radially localized region on the high-field side where the resonant condition $\omega_A(Z, R) = \omega$ is satisfied [$\omega_A(Z, R) = nV_A/R$ is the local Alfvén frequency, and ω is the frequency of the CAE mode in the simulation]. Simulations for both low-n and high-n CAEs show resonant coupling to the shear Alfvén wave. The amplitude of $\delta B_\perp$ at the resonance location is about 1.5 times larger than the amplitude of the driving compressional mode (Fig. 2). Analysis of magnetic and velocity perturbations of the resonant mode shows that its polarization is consistent with that of the kinetic Alfvén wave, namely, that δB_Z and δV_Z are the dominant components, and $\delta V_Z \sim -\delta B_Z$. The radial wavelength of the KAW is about 0.2 m, which is comparable to the beam-ion Larmor radius, $k_\perp \rho_{\text{beam}} \sim 1$. Both the CAE and the KAW are propagating in the direction of the current and the beam-ion velocity (corotating CAE), so $k_\parallel$ is positive. Also, it is known that $k_\perp$ of KAWs in a nonuniform plasma is directed towards the side with smaller Alfvén speed [17]. In toroidal geometry, this
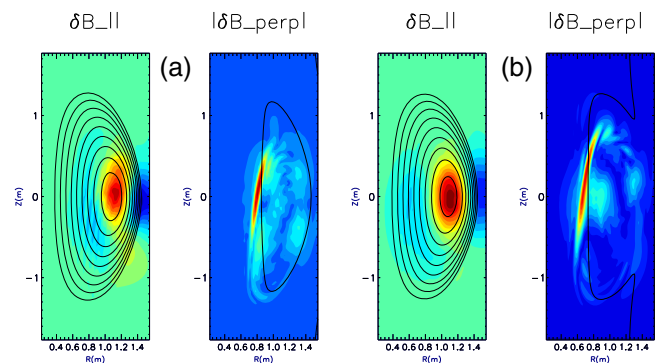

FIG. 1 (color online). Contour plots of magnetic-field perturbation for $n = 8$ (a) and $n = 4$ (b) CAE modes show resonant coupling to KAWs. The solid contour line on the $|\delta B_\perp|$ plots corresponds to the resonant condition $\omega_A(Z, R) = \omega$.
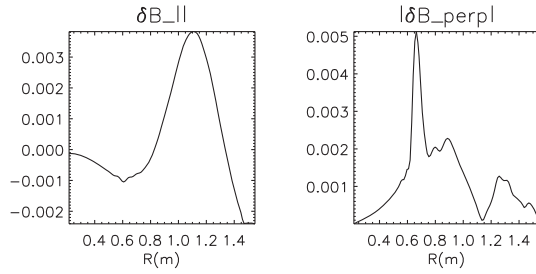
FIG. 2. Radial profiles of magnetic-field perturbation for the $n = 4$ CAE versus major radius. The CAE peaks near the magnetic axis, where $\delta B_\parallel \gg \delta B_\perp$.

results in a mode structure that is tilted relative to the magnetic flux surfaces (Fig. 1), and, since only the modes with positive $k_\parallel$ are unstable, it also results in the mode structure which is not up-down symmetric.

The coupling between the compressional Alfvén waves and KAWs near the Alfvén field-line resonance location has been studied before, both analytically and numerically, in application to space plasma physics [17–20], and to plasma heating by fast magnetosonic waves in tokamak plasmas [21–23]. It was found that the compressional wave can mode convert into a KAW with an amplitude that is enhanced compared to that of the driving compressional wave, consistent with HYM simulation results. Hybrid simulations in a 2D box geometry investigated beam-ion-driven compressional mode conversion to KAWs [20] in nonuniform plasmas. The perpendicular scale length of the KAW was found to be determined by the ion Larmor radius, and the polarization of the KAW and the tilting of its wave front relative to the background magnetic field are consistent with HYM simulations. Numerical simulations of the conversion of fast waves in low-aspect-ratio tokamak plasmas also found lack of up-down symmetry and high-field-side localization of the converted modes [23].

One of the distinguishing features of CAEs in toroidal geometry is that the location of the shear Alfvén resonance always coincides with the edge of an effective potential well within which the CAE is nonevanescent (Fig. 3). CAEs can be described by a simplified 2D wave equation using an effective potential [4,16] $V_{\rm eff} = -\omega^2/V_A^2 + k_\parallel^2$.
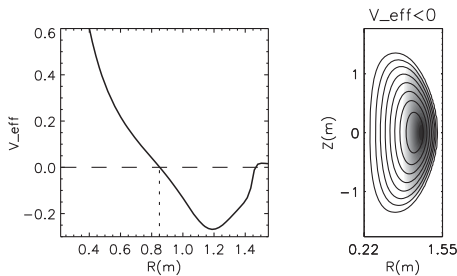

FIG. 3. Radial profile and contour plot of the effective potential $V_{\rm eff}$ for the $n = 8$ CAE with $\omega = 0.48\omega_{ci0}$. The mode can exist for $V_{\rm eff} < 0$ with radial extent 0.86 m $< R < 1.45$ m.

The radial profile and contour plot of $V_{\rm eff}$ for the $n = 8$ CAE mode with $\omega = 0.48\omega_{ci}$ are shown in Fig. 3 for $k_\parallel = n/R$. Compressional Alfvén waves can propagate for $V_{\rm eff} < 0$, but will be evanescent where $V_{\rm eff} > 0$. Radial extent of $V_{\rm eff} < 0$ is 0.86 m $< R < 1.45$ m, consistent with the mode structure shown in Fig. 1(a). The condition $V_{\rm eff} = 0$ is identical to the Alfvén resonance condition; therefore, resonance with the Alfvén continuum is located at the edge of the CAE well, leading to a strong coupling between the compressional mode and KAWs.

In the ideal MHD model, there is a logarithmic singularity at the resonance location where the CAE frequency matches the local Alfvén frequency [17]. In the HYM model, this singularity is resolved by the fast-ion finite Larmor radius effects and mode conversion to KAW; in order to demonstrate that, the dispersion relation for KAW has been derived. In the full kinetic model for a three-component plasma including the beam ions, assuming for simplicity Maxwellian ions with $V_0 = 0$, and including only an adiabatic beam ion contribution,

$$\omega^2 = k_\parallel^2 V_A^2 \left(1 + \lambda_e + \frac{3}{4}\frac{n_i}{n_e}\lambda_i + \frac{3}{4}\frac{n_b}{n_e}\lambda_b - \frac{\omega^2}{\omega_{ci}^2} \right),$$
$$\text{where } \lambda_\alpha = \frac{k_\perp^2 T_\alpha}{m_i \omega_{ci}^2} \tag{4}$$

and it was assumed that $\lambda_\alpha < 1$ and $\omega < \omega_{ci}$. This is the well-known KAW dispersion relation modified by the beam-ion effects. Repeating the same derivation with the HYM model assumptions, we obtain

$$\omega^2 = k_\parallel^2 V_A^2 \left(1 + \frac{3}{4}\frac{n_b}{n_e}\lambda_b - \frac{n_b}{n_e}\frac{\omega^2}{\omega_{ci}^2} \right), \quad \lambda_b = \frac{k_\perp^2 T_b}{m_i \omega_{ci}^2}, \tag{5}$$

which is consistent with the full kinetic result in the limit $\lambda_e \to 0$, $\lambda_i \to 0$, and $\omega \ll \omega_{ci}$. Since the numerical model treats the thermal plasma as a MHD fluid, the KAW perpendicular scale is determined by the beam-ion finite Larmor radius effects, as demonstrated by the simulation results. The HYM simulation model does not include the kinetic electrons and transit-time magnetic pumping effects. Estimates show that related damping is small compared to the Alfvén resonance damping, because all unstable CAE modes in our simulations have relatively large-$k_\parallel$ and low-poloidal mode numbers. This is the limit opposite to that considered by Mahajan and Ross [8]. Estimates for the $n = 8$ CAE mode give $\omega/k_\parallel v_{th,e} \sim 0.1$ and $\text{Im}(\omega)/\omega \sim 0.04\beta_e \sim 0.004$. However, these damping mechanisms could still be important in the nonlinear regime, and they might be responsible for the lower observed saturation amplitudes compared to those calculated numerically.

The condition $k_\perp \rho_b \sim 1$ implies that the ion and electron motions are decoupled in KAWs, leading to the generation
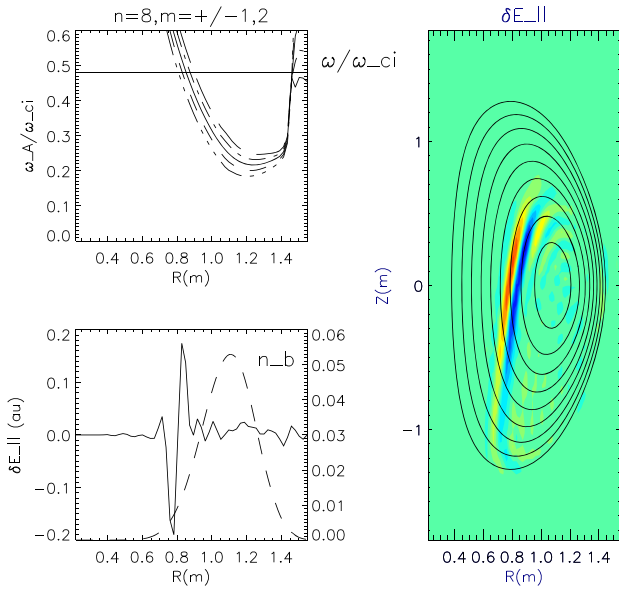
FIG. 4 (color online).　Radial profile of Alfvén continuum, $\delta E_\parallel$ and beam-ion density profile, and contour plot of $\delta E_\parallel$ for the $n = 8$ CAE mode.

of finite parallel electric-field perturbations, which is typical for KAWs. Figure 4 shows the radial profile and poloidal contour plot of $\delta E_\parallel$ obtained in simulations of the $n = 8$ CAE/KAW instability. It is seen that the $\delta E_\parallel$ location and poloidal structure is related to the KAW, whereas the CAE has an ideal MHD character with negligible $\delta E_\parallel$.

Numerical simulations presented here demonstrate that a resonant mode conversion of CAE to kinetic Alfvén waves will occur for any unstable CAE in NSTX or other toroidal devices, independent of toroidal mode number or mode frequency. The strong CAE/KAW coupling supports an alternative mechanism for T_e flattening, in which beam-driven CAE dissipates its energy at the resonance location with KAW, thereby significantly modifying the energy deposition profile (similar to a mechanism suggested qualitatively in [10]). Figure 5 shows the radial profile of the radial component of the Poynting vector $S_R = \langle \mathbf{E} \times \mathbf{B} \rangle_R$ obtained from self-consistent nonlinear simulations of the $n = 4$ CAE mode near saturation. It is seen that the energy flux is directed away from the magnetic axis (CAE) towards
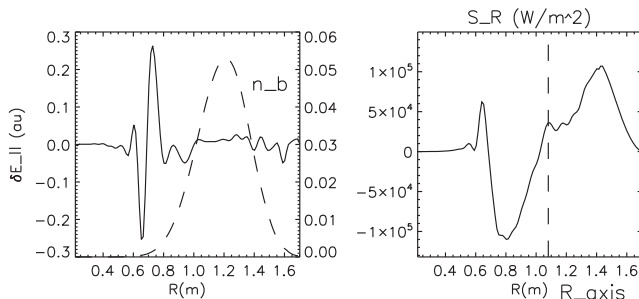

FIG. 5.　Radial profiles of $\delta E_\parallel$ and radial component of Poynting vector $S = \langle E \times B \rangle$ for the $n = 4$ CAE mode.

the Alfvén resonance location (KAW). The calculated change of the energy flux across the resonant layer at $R = 0.6$–0.7 m is 1.5×10^5 W/m^2, and, estimating the surface area as $\sim$2–3 m^2, the power absorption can be calculated as 0.3–0.5 MW, which is a significant fraction of the beam power. The saturation amplitude of the $n = 4$ CAE instability in the simulations is $\delta B_\parallel / B_0 = 6.6 \times 10^{-3}$, which is comparable to values obtained by analyzing experimental data from the same NSTX shot. Thus, measured plasma displacement $|\xi| = 0.1$–0.4 mm [C13] corresponds to $\delta B_\parallel / B_0 = (0.9$–$3.4) \times 10^{-3}$, where the HYM-calculated mode structure was used to relate displacement and magnetic-field perturbation amplitudes. It is also useful to estimate a fraction of beam power that can be transferred to CAE as $P = 2\gamma \int (\delta B)^2 / 4\pi d^3 x$. For $\gamma / \omega_{ci} = 0.005$–$0.01$ and experimentally measured amplitudes, it gives $P = (0.013$–$0.4)$ MW, comparable to the absorption rate obtained in nonlinear simulations. The calculations demonstrate that a significant fraction of beam energy can be transferred to several unstable CAEs of relatively large amplitudes and dissipated at the resonant location via electron Landau damping. The calculated power absorption is significant enough to have a direct effect on the electron temperature profile.

In addition, radially overlapping KAWs can strongly enhance plasma heat transport due to finite $\delta E_\parallel$. Previous studies have shown that addition of the finite parallel electric field to the ideal GAE structure has a strong effect on the electron transport [9]. Our simulations show that the radial width of KAWs can be comparable to the beam-ion Larmor radius, which is relatively large for 90-keV beams in NSTX. Therefore, in cases when several CAEs are observed, the KAWs will likely overlap radially. For example, for the $n = 8$ and $n = 4$ CAEs considered here, the KAWs overlap significantly, as can be seen from radial profiles of $\delta E_\parallel$ in Figs. 4 and 5. Several overlapping KAWs with relatively large $\delta E_\parallel$ can have a direct effect on both the electron transport and the beam-ion redistribution.

In summary, it is found that beam-driven compressional Alfvén modes in NSTX mode convert to KAWs, and, therefore, can channel the energy of the beam ions from the injection region near the magnetic axis to the location of the resonant mode conversion at the edge of the beam density profile. This mechanism can provide an alternative explanation to the observed reduced heating of the plasma center in the NSTX. A detailed description of nonlinear simulation results and comparisons of the relative importance of the energy-channeling and anomalous electron-transport mechanisms will be reported in future publications.

*ebelova@pppl.gov

[1] D. Stutman, L. Delgado-Aparicio, N. Gorelenkov, M. Finkenthal, E. Fredrickson, S. Kaye, E. Mazzucato, and K. Tritz, Phys. Rev. Lett. **102**, 115002 (2009).

[2] N. A. Crocker, E. D. Fredrickson, N. N. Gorelenkov, W. A. Peebles, S. Kubota, R. E. Bell, A. Diallo, B. P. LeBlanc, J. E. Menard, M. Podesta, K. Tritz, and H. Yuh, Nucl. Fusion **53**, 043017 (2013).

[3] E. D. Fredrickson, N. Gorelenkov, C. Z. Cheng, R. Bell, D. Darrow, D. Johnson, S. Kaye, B. LeBlanc, J. Menard, S. Kubota, and W. Peebles, Phys. Rev. Lett. **87**, 145001 (2001).

[4] N. N. Gorelenkov, E. Fredrickson, E. Belova, C. Z. Cheng, D. Gates, S. Kaye, and R. White, Nucl. Fusion **43**, 228 (2003).

[5] S. M. Mahajan, D. W. Ross, and G. L. Chen, Phys. Fluids **26**, 2195 (1983).

[6] S. M. Mahajan, Phys. Fluids **27**, 2238 (1984).

[7] Y. M. Li, S. M. Mahajan, and D. W. Ross, Phys. Fluids **30**, 1466 (1987).

[8] S. M. Mahajan and D. W. Ross, Phys. Fluids **26**, 2561 (1983).

[9] N. N. Gorelenkov, D. Stutman, K. Tritz, A. Boozer, L. Delgado-Aparicio, E. Fredrickson, S. Kaye, and R. White, Nucl. Fusion **50**, 084012 (2010).

[10] Y. I. Kolesnichenko, Y. V. Yakovenko, and V. V. Lutsenko, Phys. Rev. Lett. **104**, 075001 (2010).

[11] E. V. Belova, S. C. Jardin, H. Ji, M. Yamada, and R. Kulsrud, Phys. Plasmas **7**, 4996 (2000).

[12] E. Belova, N. Gorelenkov, C. Cheng, and E. D. Fredrickson, in *Proceedings of the 30th EPS Conference on Controlled Fusion and Plasma Physics, St. Petersburg, Russia, 2003* (European Physical Society, St. Petersburg, Russia, 2003), Vol. 27A, p. 3.102.

[13] E. Belova, N. Gorelenkov, E. Fredrickson *et al.*, in *Proceedings of the 24th IAEA Fusion Energy Conference, San Diego, CA, 2012* (International Atomic Energy Agency, Vienna, 2012).

[14] E. Belova, N. Gorelenkov, and C. Cheng, Phys. Plasmas **10**, 3240 (2003).

[15] N. A. Crocker *et al.*, in *Proceedings of the 24th IAEA Fusion Energy Conference, San Diego, CA, 2012* (International Atomic Energy Agency, Vienna, 2012).

[16] E. D. Fredrickson, N. N. Gorelenkov, M. Podesta *et al.*, Phys. Plasmas **20**, 042112 (2013).

[17] A. Hasegawa and L. Chen, Phys. Fluids **19**, 1924 (1976).

[18] J. R. Johnson and C. Z. Cheng, Geophys. Res. Lett. **24**, 1423 (1997).

[19] Y. Lin, J. R. Johnson, and X. Y. Wang, J. Geophys. Res. **115**, A04208 (2010).

[20] M. H. Hong, Y. Lin, and X. Y. Wang, Phys. Plasmas **19**, 072903 (2012).

[21] C. F. F. Karney, F. W. Perkins, and Y.-C. Sun, Phys. Rev. Lett. **42**, 1621 (1979).

[22] J. A. Heikkinen, T. Hellsten, and M. J. Alava, Nucl. Fusion **31**, 417 (1991).

[23] K. Kommoshvili, S. Cuperman, and C. Bruma, Plasma Phys. Controlled Fusion **45**, 275 (2003).